

Serial No. 10/761,076

Docket No. 145523-1

REMARKS

Applicants appreciate the consideration shown by the Office as evidenced by the Office Action mailed on June 23, 2005. In that Office Action, the Examiner rejected claims 1-31. In this Response, Applicants have amended claims 1, 13, and 23; and have canceled claims 4, 16, and 25. Claims 1-3, 5-15, 17-24, and 26-74 remain pending in this application, with claims 32-74 currently withdrawn from consideration on the basis of a restriction requirement. Applicants respectfully request favorable reconsideration in light of the above amendments and the following remarks.

1. Claim Rejections

Claims 1-31 were rejected under 35 U.S.C. 102 (a) or (e) as anticipated by, or, in the alternative, under 35 U.S.C. 103(a) as obvious over Asakawa et al., U.S. Patent No. 6,565,763 ("Asakawa"). Applicants respectfully traverse this rejection.

Asakawa does not anticipate independent claims 1, 13, and 23 of the present application as amended herein because this applied reference does not describe or imply a ceramic material having a porosity of less than 30 percent. Moreover, the subject matter recited by claims 1, 13, and 23 of the present application, taken as a whole, is not obvious in view of Asakawa because this applied reference fails to suggest a ceramic material having porosity less than 30 percent. First, Asakawa is silent on the issue of the porosity range of the material made by its disclosed process. No specific values are given, and the word "porosity" is not present in the reference. Second, Asakawa makes very clear that the invention it describes is directed to the production of materials having a high level of porosity. In column 6, lines 10-15, the very beginning of the Detailed Description section, Asakawa states, "The principle of the present invention is that a film or a bulk-molded product of a block copolymer or graft copolymer is formed, which copolymer is allowed microphase-separation, and then a polymer phase is selectively removed, thereby forming a porous film or porous structure having a pattern of the order of nanometers." Moreover, the porous structures must have a high porosity, because "such a structure [formed by the disclosed process] has a very large specific surface area. Col. 14, lines 34-37.

The stark differences between the materials described in Asakawa and those claimed in the present application arise because Asakawa and the present application describe two very

Serial No. 10/761,076

Docket No. 145523-1

different processes. In Asakawa, a block copolymer is forced to undergo micro-phase separation, and then one of the separated phases is selectively removed, leaving behind a structure comprising the remaining phase and a high level of porosity disposed where the removed phase previously resided. Column 6, lines 10-15. On the other hand, in the present application, a block copolymer (BCP) is mixed with at least one ceramic precursor. The mixture assembles into an ordered structure, but in this case there is no phase separation of the BCP with selective removal of a constituent BCP phase; instead, the mixture is pyrolyzed to decompose at least a portion of the BCP, leaving behind carbonaceous material (paragraph 0032). As noted in paragraph [0028] of the present specification, "Voids left behind by the decomposition of block copolymer can be closed during pyrolysis, leading to a nonporous, dense material." As noted above, Asakawa is clearly directed at just the opposite result—the production of porous material.

Based on the above discussion, Applicants respectfully submit that independent claims 1, 13, and 23, along with their respective pending dependent claims, are patentably distinct from Asakawa. Applicants respectfully request favorable reconsideration of the claims.

2. Information Disclosure Statement (IDS)

The Examiner stated that the IDS filed 1-16-04 failed to comply with 37 C.F.R. 1.98(a)(2) because documents C3 and C4 were not received. Reference C3 is Monnier et al., "Cooperative Formation of Inorganic – Organic Interfaces in the Synthesis of Silicate Microstructures," *Science*, vol. 261, pp. 1299-1303, September 3, 1993. Reference C4 is Templin et al., "Organically Modified Aluminosilicate Mesostructures from Block Copolymer Synthesis," *Science*, vol. 278, pp. 1795-1798, December 5, 1997.

Applicants enclose herein copies of the two references, and respectfully request consideration of all disclosed references.

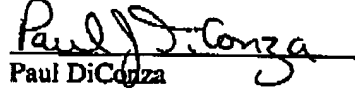
Serial No. 10/761,076

Docket No. 145523-1

3. Conclusion

In light of the remarks and amendments presented herein, Applicants believe that this serves as a complete response to the subject Office Action. If, however, any issues remain unresolved, the Examiner is invited to telephone the undersigned at the number provided below.

Respectfully submitted,



Paul DiCorza

Reg. No. 48,418

General Electric Company

Building K1, Room 3A60

Telephone: (518) 387-6131

1 Research Circle
Niskayuna, New York
Friday, September 23, 2005

Attachments: 2 journal articles as noted above

PORTS

Cooperative Formation of Inorganic-Organic Interfaces in the Synthesis of Silicate Mesosstructures

Donnier, F. Schüth, Q. Huo, D. Kumar, D. Margoese, Maxwell, G. D. Stucky,* M. Krishnamurty, P. Petroff, A. Firouzi, M. Janicke, B. F. Chmelka

presented to explain the formation and morphologies of surfactant-silicate mesosstructures. Three processes are identified: multidentate binding of silicate oligomers to surfactant, preferential silicate polymerization in the interface region, and charge density matching between the surfactant and the silicate. The model explains experimental data, including the transformation between lamellar and hexagonal mesosstructures, and provides a guide for predicting conditions that favor the formation of lamellar, hexagonal, or cubic mesosstructures. Model Q²³⁰ proposed by Mariani and his co-workers satisfactorily fits the x-ray data collected on the cubic mesostructure material. The model suggests that the silicate polymer forms a unique infinite silicate sheet sitting on a minimal surface and separating the surfactant molecules into two disconnected regions.

Discovery of a new family of mesoporous materials, designated M41S, by scientists at the Mobil Oil Corporation (1), has dramatically extended the range of crystalline pore sizes from the microporous (less than 10 Å) to the mesopore (20 to 100 Å). The synthesis uses ordered arrays of surfactant molecules as a "template" for the polymerization of silicates. These materials obtained by this process have several remarkable features: (i) large pore sizes and shape, as compared to microporous materials; (ii) fine adjustment of pore size within the limits stated above; (iii) high thermal and hydrolytic stability; and (iv) a very high degree of ordering over micrometer distances. These unusual properties are a result of the interplay between organization of the surfactant molecules and polymerization of the silicate in the aqueous phase.

(2) outlined two general models for the formation of the mesoporous materials. The first model assumes that the surfactant is the structure-directing element in the synthesis of the liquid crystal phase. The second model suggests that the addition

of the silicate orders the subsequent silicate-encased surfactant micelles. These general models, however, are insufficient for establishing the mechanistic understanding needed for better control of the synthesis process, which is key to efforts aimed at improving or adding to this exciting new class of materials. On the basis of experimental results, we present here a more detailed model of the mesophase formation process, which explains presently known experimental data and successfully predicts conditions needed for the synthesis of desired structures. We believe that this model can be generalized to the synthesis of other nonsiliceous materials as well.

From considerations in surfactant and silicate chemistry, three closely coupled phenomena are identified as crucial to the formation of surfactant-silicate mesophases. These include: (i) multidentate binding of silicate oligomers, (ii) preferred polymerization of silicates at the surfactant-silicate interface, and (iii) charge density matching across the interface.

Mesostructure syntheses can be carried out under conditions in which the silicate alone would not condense (at pHs from 12 to 14 and silicate concentrations of 0.5 to 5%) and the surfactant cetyltrimethylammonium (CTA⁺) alone would not form a liquid crystal phase. In fact, surfactant-silicate mesophases can form at surfactant concentrations as low as 1%, a regime in the CTABr-water phase diagram in which only micelles are present. For a CTABr-water solution at typical surfactant-silicate synthesis temperatures in the absence of silicates, a hexagonal phase is favored at surfactant concentrations from ~25 to 70% by weight whereas a lamellar phase forms at concentrations above 70% (3, 4). Never-

theless, a solid mesophase precipitate is formed, the structure of which will be discussed below, as soon as surfactant (chain length of 8 to 20 carbon atoms) and silicate solutions are combined. The rapidity of this precipitation indicates that there is a strong interaction between the cationic surfactant and anionic silicate species in the formation of surfactant-silicate mesophases.

We performed syntheses aimed at identifying conditions important for the formation of mesoporous materials over a wide range of reactant compositions and temperatures (5). For the purpose of investigation, we found that we could slow the evolution of the surfactant-silicate systems by undertaking the syntheses at moderate temperatures (between 30° and 100°C) (6). During freeze-dry kinetic experiments with CTACl used as the surfactant, a layered (lamellar) material with a primary *d* spacing (repeat distance) of 31(±1) Å was produced, together with amorphous silica, after reaction times on the order of 1 min. For the synthesis conditions given in Fig. 1, the lamellar mesophase disappears after approximately 20 min, at which point the diffraction pattern of the hexagonal mesostructure is simultaneously detected. This hexagonal material has a primary *d* spacing of 40(±1) Å and attains its final degree of ordering after ~10 hours (7).

A layered material with a primary *d* spacing of 31(±1) Å (Fig. 2, pattern A) can be isolated in pure form (8); a transmission electron microscopy (TEM) micrograph of this mesostructure is depicted in Fig. 3. The variation of the *d* spacing as a function of the chain length of a cationic surfactant C_nH_{2n+1}(N(CH₃)₃)⁺ (for 14 ≤ *n* ≤ 22) is 1.0 to 1.2 Å per carbon, which

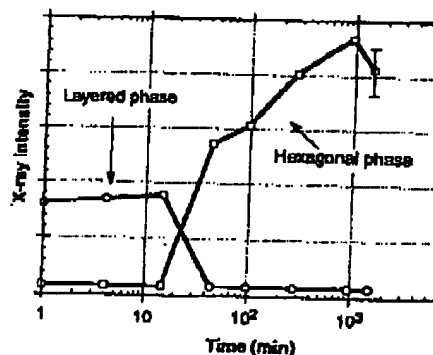


Fig. 1. Time evolution of the intensity of x-ray diffraction features associated with layered and hexagonal (M41S) mesostructures at 348 K. The layered material is precipitated rapidly, whereas the hexagonal material appears later, as a result of a higher degree of silica polymerization. The composition of the reaction mixture was as follows: 1 M SiO₂:0.025 M Al₂O₃:0.115 M Na₂O:0.233 M CTACl:0.089 M TMAOH:125 M H₂O.

Department of Chemistry, University of California, Santa Barbara, CA 93106, and Département de Chimie, Université de Genève, CH-1211 Geneva, Switzerland.

Department of Chemistry, University of California, Santa Barbara, CA 93106, and Institut für Chemie, Johannes-Gutenberg-Universität, D-55128 Mainz, Germany.

D. Margoese, R. S. Maxwell, G. D. Stucky, Department of Chemistry, University of California, Santa Barbara, CA 93106.

P. Petroff, Materials Department, University of California, Santa Barbara, CA 93106.

M. Janicke, B. F. Chmelka, Department of Chemical Engineering, University of California, Santa Barbara, CA 93106.

* To whom all correspondence should be addressed.

corresponds to a monolayer assembly. If this new layered material is hydrothermally treated at 373 K (pH = 7), it is converted to the hexagonal mesostructure over 10 days, with intermediate and final x-ray patterns shown in Fig. 2, patterns B and C, respectively. During this transformation the degree of silica polymerization increases, as measured by the relative number of incompletely condensed (Q^3) and fully condensed (Q^4) silicon atoms determined by ^{29}Si magic-angle spinning nuclear magnetic resonance spectroscopy. The ratio between Q^3 and Q^4 silicon decreases from typical values of 1.0 for the layered material to 0.4 to 0.55 for the hexagonal mesostructure, reflecting a significant increase in the number of silicon atoms fully coordinated to other silicate nearest neighbors.

Mesophase formation and associated silica polymerization are intimately tied to Coulombic interactions between surfactant and silicate species at the micelle interfaces. Silicates present in the form of monovalent monomers, $\text{Si}(\text{OH})_3\text{O}^-$, however, are expected to have little energetic advantage over other monovalent anions competing for access to the cationic surfactant head groups. At high pH, the reaction mixture also contains small silica oligomers (three to seven silicon atoms) of varying degrees of polymerization and charge (9). These oligomers are appreciably more acidic ($\text{p}K_a \sim 6.5$) than the monomer or dimer species [$\text{p}K_a$ 9.8 and 10.7, respectively (10)], although all such silicates will be highly dissociated under the high pH conditions used here (11).

The oligomeric silica polyanions, however, can easily act as multidentate ligands for the cationic head groups of the surfactant, leading to a strongly interacting surfactant-silicate interface. Indeed, the interaction of ionic surfactants with polyions of opposite charge encourages strong cooperative binding, manifested by increases in the binding constants of up to two orders of

magnitude in similar systems (12). Preferential multidentate binding of the silicate polyanions causes the interface to quickly become populated by tightly held silicate oligomers, which can subsequently polymerize further. Silicate polymerization within the surfactant-silicate interface region is favorable for two related reasons: (i) the concentration of silicate species near the interface is high and (ii) their negative charges are partially screened by the surfactant. Furthermore, as polymerization proceeds, the formation of highly connected silicate polyanions, which act as very large multidentate ligands, further enhances the cooperative binding between the surfactant and silicate species.

Multidentate ionic binding in surfactant-silicate systems has an important consequence; namely, it leads to precipitation of a given mesophase from solution. Through the interactions driving the precipitation process, the appearance of a given mesostructure is established, although this process is expected to operate on a different time scale from polymerization of the silica, which accounts ultimately for the thermal, mechanical, and hydrolytic stability of the final material. If small silica oligomers are present in sufficient quantity, precipitation of the surfactant-silicate system is primarily the result of electrostatic interactions, combined with packing constraints associated with the hydrophobic surfactant chains. Whereas precipitation is fast and essentially thermodynamically controlled, silica polymerization into a strong and extended framework is slow and reaction rate-limited. This two-stage process is in agreement with experimental findings that contrast the mesostructures obtained at room temperature after short reaction times with those obtained at high temperature after long reaction times: very similar x-ray patterns are obtained for both sets of conditions, indicating identical precipitated mesostructures; however, the materials syn-

thesized by the low-temperature thermally and mechanically stable than the high-temperature coupling between the polymerization processes in silicate systems provides the mellar-to-hexagonal mesostructure in a way that we now discuss.

The resemblance, in the surfactant-silicate mesostructures, to the corresponding water-soluble crystal phases indicates that the interactions responsible for these phases are of a similar nature. The head-group area (A) in a particular mesophase is recognized in water-soluble favored mesophase is that to be closest to its optimal, maintaining favorable packing of hydrophobic surfactant chains. In surfactant-silicate systems, the packing is strongly affected by electrostatic interactions between the silicate and surfactant micelle species. More precisely, its value is obtained by minimizing the Gibbs free energy G as a function of

$$A_0 \rightarrow (\partial G / \partial A) = 0$$

$$G(A, \rho) = G_{\text{inter}}(A) + G_{\text{wall}}(A) + G_{\text{sol}}(A, \rho) + G_{\text{elec}}(A, \rho)$$

where G_{inter} reflects the forces and conformational entropy of hydrocarbon chains and their interactions with the head group within a single micelle; G_{wall} counts for the polysilicate energy, including the solvent and silicate van der Waals and electrostatic interactions within the micelle framework or "wall"; G_{sol} describes the interactions with wall-micelle and micelle-micelle interactions; G_{elec} describes the phase; and ρ specifies the chemical potentials of the species in the aqueous solution, as defined for by G_{sol} .

Fig. 2. Powder x-ray diffraction patterns of surfactant-silicate mesostructures precipitated from the same reaction mixture (1 M SiO_2 ; 0.034 M Al_2O_3 ; 0.07 M Na_2O ; 0.27 M CTABr; 0.14 M TMAOH; 0.28 M TMB; 100 M H_2O), and then treated hydrothermally at 373 K for different times. X-ray patterns are shown for (curve A) the initially precipitated layered material, (curve B) an intermediate material, and (curve C) the M41S hexagonal mesostructure acquired 0, 1, and 10 days, respectively, after initiation of the hydrothermal treatment.

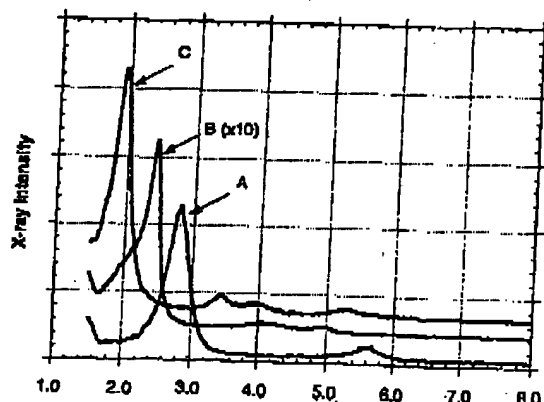


Fig. 3. Transmission electron micrograph of the layered surfactant-silicate mesostructure whose x-ray data are shown in Fig. 2.

structure, roughly spherical micelle shape for a given surfactant concentration A and is also responsible for the swelling of the micelles when "expanders," such as trimethylamine (TMA) are added to the solution. The term G_{wall} drives the chemistry of the wall, including the polymerization of silicate species, and contains the structural information responsible for the multidentate interactions between A and the state of the wall. The term G_{inter} establishes the coupling between A and the state of the wall by p . This coupling across the interface can be understood in terms of electrostatic interactions (which most likely dominate), whereby the silicate density within the wall, ρ_s , is much higher than the density of the surfactant groups, which have an average charge density of $1/A$. Thus, the electrostatic interactions link A_0 , as defined by ρ_s , with p , a relation we refer to as "density matching." Such interdependent electrostatic effects control the distribution of surfactant intercalates in different silicate types (15) and have been used to explain the "self-replication" of silica layers in purely inorganic systems (16).

In surfactant-silicate systems, polymerization driven by G_{wall} will profoundly affect the mechanism to explain the transition between the lamellar and hexagonal

mesophases. In the early stage of the synthesis, the presence of highly charged silica oligomers favors a small value of A_0 , which can be achieved with a lamellar surfactant configuration. As rearrangement and polymerization of the silicate species proceed, the density of anionic silanol groups diminishes, so that A_0 increases, while the number of compensating cations decreases. At the same time, the wall thickness can decrease from its initial value without energy cost, because the most stable ionized silanol groups are confined to the wall surface, thus reducing repulsive dipole-dipole interactions between the two opposite-facing wall surfaces. The silicate wall is still poorly condensed during early stages of the synthesis, allowing the system to increase its A toward A_0 by adopting the hexagonal structure according to charge-density matching criteria. Under these circumstances, the wall thickness simultaneously decreases to keep the volume ratio CTA/SiO₂ constant. The actual wall thickness has been estimated to be 10 to 11 Å (17) for the lamellar mesophase and 8 to 9 Å (18) for the hexagonal mesophase. Simple geometrical arguments can be used to show that these values are consistent with a constant CTA/SiO₂ volume ratio throughout the phase transition.

The regularity of the product mesostructures supports mediation of the silicate wall

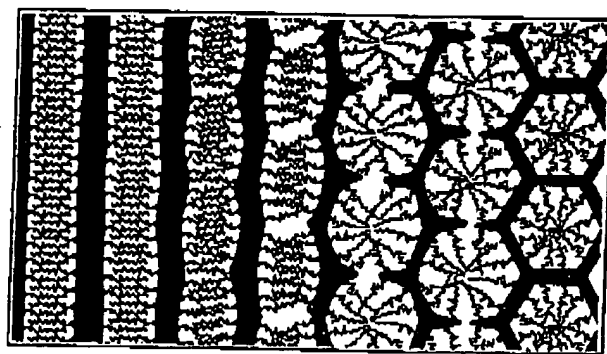
thickness during the assembly process. The high efficiency of this mediation is reflected in the experimental observation that the wall thickness of the hexagonal phase is essentially constant (8 to 9 Å) over a wide range of reaction conditions, independent of the surfactant chain length, and by the clearly hexagonal, as opposed to circular, pore shape established by both high-resolution TEM and modeling of the powder x-ray diffraction patterns (19). Control of the silicate wall thickness is undoubtedly related to the double layer potential: silicate species are only accumulated at the surfactant interface to the extent necessary for charge compensation. Polymerization normal to the interface, which would thicken the wall or produce amorphous bulk SiO₂, does not occur because of the strong electrostatic repulsion produced by the high negative charge on the silicate species at pH 12 and above (10).

Figure 4 shows a mechanism consistent with current experimental investigations by which the lamellar-to-hexagonal mesophase transformation may occur. Silica polymerization leads to an increase in interfacial area that is achieved through corrugation of the lamellar surfactant-silicate sheets. As implied in the final step, this corrugation progresses until connection between the sheets is made at the cusps, resulting ultimately in the formation of the hexagonal mesophase. Another way to accommodate the change in A would be to maintain a planar structure while tilting the hydrocarbon chains. Such a transition, however, is entropically disfavored by the restrictive chain configuration this suggests.

Yanagisawa *et al.* (20) recently reported a hexagonal mesostructure, with pore dimensions similar to that of M41S, produced by the inclusion of CTA⁺ cations into the sheet silicate kanemite. During their synthesis these researchers observed a layered intermediate that subsequently transformed into a hexagonal phase material. This process is probably driven by the same forces as the transformation we report, although it is not yet clear to what extent the kanemite structure is preserved during the conversion. If the pH is sufficiently basic, for example, the sheets can be partially or fully destroyed during the process.

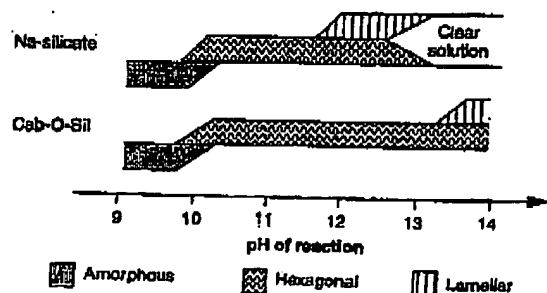
We propose that the surfactant-silicate mesophase structure is governed primarily by the terms G_{inter} and G_{wall} of Eq. 2. In this respect, the main effect of the silicate wall and of the reaction conditions are to determine A_0 . This provides predictive capability for establishing the reaction conditions that favor the lamellar or the hexagonal mesophases. We have tested this model experimentally by monitoring the effects of pH and the degree of polymerization of the silica source on the mesostructure synthesized in Fig.

A schematic diagram illustrating the mechanism proposed for the transformation of the surfactant-silicate system from the lamellar to the hexagonal mesophase. The diagram shows the progression of the system as a function of pH, with the surfactant-silicate sheets becoming increasingly corrugated and eventually forming a hexagonal network.



SiO₂ Reaction coordinate

showing the approximate mechanism of formation of the hexagonal surfactant-silicate mesophase, as functions of silica source, Cab-O-Sil 100 Å oligomeric silicate, whereas Na-silicate is a source of hydrolyzed and oligomeric silicates.



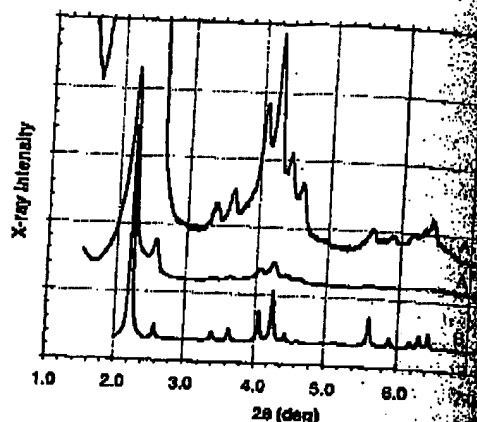
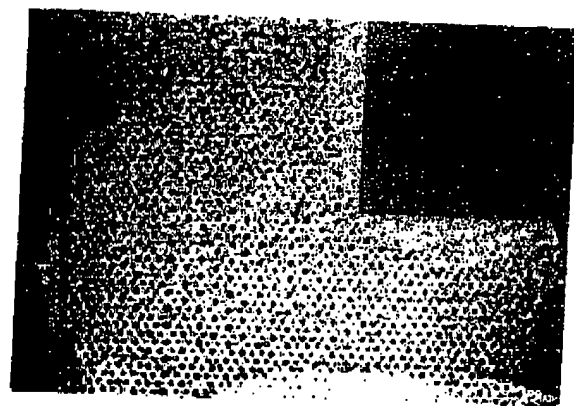


Fig. 6 (left). Transmission electron micrograph of the cubic surfactant-silicate mesostructure showing an ordered ~ 2000 Å aggregate viewed along its [111] axis. Fig. 7 (right). X-ray powder diffraction pattern of the cubic mesostructure, with $Ia3d$ symmetry, synthesized from a reac-

tion mixture with a molar composition of 1 M TEOS:0.25 M CTACl:62 M H_2O for 3 days at 373 K (curve A). Calculated pattern using the Q^{230} model proposed by Mariani *et al.* (21) parameter $a = 97.3$ Å (curve B).

5. These results lead to the following conclusions in accordance with our predictions:

1) The lamellar phase is favored at high pH and for a low degree of polymerization of the silica source.

2) The hexagonal phase is favored at low pH and for a highly polymerized silica source.

In addition, we investigated the influence of the ionic strength on the surfactant-silicate assembly process by performing the synthesis in a reaction solution also containing 1 M NaCl. The presence of the salt decreased the regularity of the material, as reflected by a reduction in the number of peaks in the x-ray pattern (from four to two). This effect, expected only at high ionic strengths, is attributed to perturbation of the double layer potential. The strong binding constant of silicate species compared to other ions makes this effect negligible at lower ionic strengths and explains why mesostructure syntheses are relatively insensitive to other counterions in the reaction mixture.

The existence of the cubic mesophase described by Beck *et al.* (2) is strongly supportive of the important role of $G_{\text{inter}} + G_{\text{inter}}$ in the formation of surfactant-silicate mesostructures. Indeed, there is remarkable similarity between the cubic mesophase, which we have recently synthesized and characterized, and the $Ia3d$ phase found in the water-CTABr system (4). A TEM image of the cubic mesostructure material (Fig. 6) shows an ordered ~ 2000 Å aggregate. The x-ray powder spectrum (Fig. 7) agrees very well with the model Q^{230} proposed by Mariani *et al.* (21) for water-surfactant systems. For this structure, it is appealing to conjecture that the midplane of the silicate wall sits on a gyroid periodic internal surface (22). Such a structure can be viewed as a single infinite silicate

sheet that separates the surfactant species into two equal and disconnected volumes. This so-called bicontinuous phase will be formed when the value of A_0 set by the reaction conditions is close to the value of the $Ia3d$ phase, namely, when pH and the CTA/SiO₂ ratio are high. It is advantageous for the silicate wall to occupy a periodic minimal surface, because it can maximize the wall thickness for a given CTA/SiO₂ volume fraction.

The leading role of $G_{\text{inter}} + G_{\text{inter}}$ in directing mesostructure formation provides a foundation for identifying potential replacement candidates for silicon in the synthesis of mesoporous inorganic frameworks. The principal criteria are that the inorganic component must be capable of forming flexible polyionic species, that extensive polymerization of the inorganic component must be possible, and that charge density matching between the surfactant and inorganic species has to occur. In other words, when G_{sol} plays a benign role, G_{wall} must not dominate $G_{\text{inter}} + G_{\text{inter}}$ in order that the mesostructure form.

In addition to binding efficiently to the surfactant interface, the best inorganic candidates will have a tendency to form glasses easily. Silicates are certainly a prototypic system in view of the ease with which they form oligomeric anions with varying degrees of polymerization. Other systems, however, may also fulfill these requirements, including transition metals, such as vanadium, or main group elements, such as boron, which can form polyanions and condense. One can also speculate about a reversed system in which an anionic surfactant is used to precipitate a cationic metal oxide precursor, the laurylsulfate-iron oxide system representing one candidate example.

firm the trends predicted for the synthesis of surfactant-silicate mesostructures. The qualitative model outlined above, which active binding provides an explanation for the strong interactions needed to stabilize mesophases from dilute solutions, differential polymerization of silicate in the region of the interface to give a double layer control of the reaction, and are responsible for the high regularity of surfactant-silicate mesostructures. Density matching establishes a link between the chemical composition and the silicate wall and the particular mesostructure. We hope these perspectives will stimulate experiments aimed at producing a better understanding of this exciting class of materials.

REFERENCES AND NOTES

1. C. T. Kresge, M. E. Leonowicz, J. S. Beck, *Nature* 359, 710 (1992).
2. J. S. Beck *et al.*, *J. Am. Chem. Soc.* 114, 1081 (1992).
3. R. G. Laughlin, *Surfactant Sci. Technol.* 1, 1 (1993).
4. X. Auvray, C. Petipas, R. A. L. Lattes, *J. Phys. Chem.* 93, 7453 (1989).
5. The general procedure for synthesizing structure materials is as follows: a solution containing silica and tetramethylammonium hydroxide (TMAH) and an aqueous solution containing surfactant and an optional aluminum species mixture is kept at temperature 373 K for reaction times between 1 and 3 days in either closed Teflon or stainless steel stirring and refluxing in a glass reactor. For the synthesis of the materials, we used Cab-O-Sil M-5 (Cabot Corporation, Boston, MA), an aqueous solution of 27.5% SiO₂, SiO₂/Na₂O (Cabot Corporation, Valley Forge, PA), orthosilicate (TEOS) (Aldrich, Milwaukee, WI), aluminum sources were obtained from Alumina Vista, Houston, TX, and sodium laurylsulfate (Spectrum Chemical, Gardena, CA), and primary ammonium alkyls C_nH_{2n+1}NH₂ (Aldrich, Milwaukee, WI).



2.25 M Na₂CO₃ calculated at (21) with

I for the
sostructure
ed above
in explain
needed to
ure solution
of silicate
together
the wall
gh regulat
structures
has a link
n and stru
e formati
We expect
imulate, g
reducing
ending of

ID NOTES

vicz, W. J.
159, 710 (1993)
tem. Soc.

Sci. Ser. 37
Anthoni
1458 (1993)

synthesis
allows: A
d optional
IAOH) is

ining the
ource. The
es between
n border
ass (1993)

M-6 (1993)
tion of
J. = 3.52
PA), 0.8

1, Mif
mitte (1993)
K) or 0.8
Jena, C

(CH₃)₂
and the

expression "surfactant-silicate" is used here as a comprehensive term for materials synthesized using a mixture of surfactant and silica. Regardless of the particular structure, information between the lamellar and hexagonal mesophases was observed after drying, as well as air-drying, the filtered

of trimethylbenzene (TMB) to the reaction mixture stabilizes the lamellar mesophase. Experiments have shown that the 31(±1) Å repeat distance for the layered material shown in Fig. 2 is preserved over a range of TMB concentrations between 0.5 and 3.0 M, whereas at TMB concentrations the hexagonal mesophase is the favored product. Stabilization of the lamellar mesophase likely occurs as TMB dissolved within the surfactant micelle assemblies contributes to the hydrophobic chain volume. This increase in surfactant chain volume increases the value of A_0 at the lamellar-to-hexagonal mesophase transition, according to a simple packing model (13). Thus, the mesostructural transition depicted in Fig. 2 is a consequence of hydrothermal removal of TMB from the surfactant chain assembly, combined with a decrease in A_0 . This conclusion is supported by separate experiments which show that removal of TMB to the aqueous phase inhibits the transition from a lamellar to a hexagonal mesophase.

Knights, C. T. G. Knight, W. E. Hurl, ACS Symp. Ser. 184, 79 (1982); C. T. G. Knight, R. G. W. Norrish, E. Oldfield, J. Magn. Reson. 78, 105 (1988); V. McCormick and A. T. Bell, Catal. Rev. Eng. 31, 97 (1989).

The Chemistry of Silica (Wiley, New York, 1993), p. 182.

W. G. Scherer, Sol-Gel Science (Academic Press, New York, 1990), p. 100.

W. G. Scherer and J. C. T. Kwac, Surfactant Sci. Technol. 1, 1 (1991).

W. G. Scherer and J. F. Sadoc, J. Phys. 48, 1559 (1987); N. Israelachvili (in Surfactants in Solution, M. J. Cantow and P. Bothorel, Eds., Plenum Press, 1987), vol. 4, p. 3) proposed the packing parameter $g = V/A_0\ell$, as a means of predicting the preferred configuration of a surfactant molecule, where V is the volume of the hydrophobic chain and ℓ is the characteristic length. According to this treatment, micelles will form if $g < 1/3$, cylindrical micelles if $1/3 < g < 1/2$, vesicles or bilayers if $1/2 < g < 1$, and inverted micelles if $g > 1$.

In (7), the presence of TMB in the reaction mixture can, but does not always, require a response in surfactant systems.

Clays and Clay Minerals. Proceedings of the International Conference on Clays and Clay Minerals, New York, 1961, vol. 10, p. 10.

Angew. Chem. Int. Ed. Engl. 20, 850 (1981).

The shape of the mesopores can be determined from the y intercept of a plot of d versus the number of carbon atoms for n -alkyl length surfactants, corrected for the head group diameter.

When d spacings, volumetric considerations on a measured void fraction of the material, and x-ray diffraction refinements based on cylindrical and hexagonal-prismatic-rod models.

W. G. D. Stucky, unpublished work.

W. T. Shimizu, K. Kuroda, C. Kato, J. Chem. Soc. Chem. Commun. 1990, 988 (1990).

Luzzati, H. Delacroix, J. Mol. Biol. 68, 449 (1973).

The minimal surface is the smallest surface that can be divided into two equal parts, given a fixed perimeter constraint.

W. G. D. Stucky, J. Zasadzinski (UCSB), J. Olson, J. Beck, J. Vartiuli, and J. W. G. D. Stucky for helpful discussions. This research was funded by Air Products, du Pont, the

MRL Program of the National Science Foundation under award DMR 9123048, the Office of Naval Research (G.D.S.), the NSF Science and Technology Center for Quantized Electronic Structures (grant DMR91-20007), the NSF/NY program, and

the Camille and Henry Dreyfus (B.F.C.) and through fellowships by (A.M.) and the DFG (F.S.).

26 April 1993; accepted 8 July 1993

An Unnatural Biopolymer

Charles Y. Cho, Edmund J. Moran,* Sara R. Cherry, James C. Stephans, Stephen P. A. Fodor, Cynthia L. Adair, Arathi Sundaram, Jeffrey W. Jacobs, Peter G. Schultz†

A highly efficient method has been developed for the solid-phase synthesis of an "unnatural biopolymer" consisting of chiral aminocarbonate monomers linked via a carbamate backbone. Oligocarbonates were synthesized from *N*-protected *p*-nitrophenyl carbonate monomers, substituted with a variety of side chains, with greater than 99 percent overall efficiencies per step. A spatially defined library of oligocarbonates was generated by photochemical methods and screened for binding affinity to a monoclonal antibody. A number of high-affinity ligands were then synthesized and analyzed in solution with respect to their inhibition concentration values, water/octanol partitioning coefficients, and hydrolytic stability. These and other unnatural polymers may provide new frameworks for development and for testing theories of protein and peptide folding and structure.

Polypeptides have been the focus of considerable attention with respect to their structure and folding, biological function, and therapeutic potential. The development of efficient solid-phase methodology for the synthesis of peptides (1), peptide derivatives (2), and large peptide libraries (3-6) has greatly facilitated these studies. The development of efficient methods for the synthesis of unnatural biopolymers (9-11) composed of building blocks other than amino acids may provide new frameworks for generating macromolecules with novel properties. For example, polymers with improved pharmacokinetic properties (such as membrane permeability and biological stability) might facilitate drug discovery, and polymers with altered conformational or hydrogen-bonding properties may provide increased insight into biomolecular structure and folding. We report the highly efficient solid-phase synthesis of oligocarbonate polymers from a pool of chiral aminocarbonates and the synthesis and screening of a library of oligocarbonates for their ability to bind a monoclonal antibody (mAb).

The oligocarbonate backbone (Fig. 1), in contrast to that of peptides, consists of a chiral ethylene backbone linked through relatively rigid carbamate groups. The α carbon, like that of peptides, is substituted

with side chains that contain a variety of functional groups. Although the β carbon is unsubstituted in our initial target, additional backbone modifications (and conformational restriction) can be incorporated via alkylation of the β carbon or the γ carbon. Oligocarbonates were synthesized from a pool of optically active *N*-protected aminocarbonates (Fig. 2), which, in turn, were derived from the corresponding optically active amino alcohols. The latter are either commercially available or can be prepared in chiral form by reduction of the *N*-hydroxysuccinimide or pentafluorophenyl esters of *N*-protected amino acids (12). The α -amino group was protected with the use of either nitroveratryl chloroformate (13) (NVOC-Cl) (for photochemical deprotection) or fluorenylmethyl-*N*-hydroxysuccinimidyl carbonate (Fmoc-OSu) (for base-catalyzed deprotection) (14). When necessary, side chains were protected as acid-labile *tert*-butyl esters, ethers, or carbamates. Protected amino alcohols were converted to the corresponding *N*-protected *p*-nitrophenyl carbonate monomers by reaction with *p*-nitrophenyl chloroformate in pyridine/CH₂Cl₂, generally in >80% yield. The carbonate monomers are stable for months at room temperature.

Solid-phase synthesis of oligocarbonates involves the sequential base-catalyzed or light-dependent deprotection of the α -amino group of the growing polymer chain followed by coupling to the next protected *p*-nitrophenyl carbonate monomer (Fig. 2). The *N*-protected "hydroxy-terminal" residue was covalently attached to polystyrene resin containing

C. Y. Cho, E. J. Moran, S. R. Cherry, J. C. Stephans, P. G. Schultz, Department of Chemistry, University of California, Berkeley, Berkeley, CA 94720.
S. P. A. Fodor, C. L. Adams, A. Sundaram, J. W. Jacobs, Affymax Research Institute, 4001 Miranda Avenue, Palo Alto, CA 94304.

*Present address: Ontogen Corporation, 2325 Camino Vida Roble, Carlsbad, CA 92009.

†To whom correspondence should be addressed.

most weakly coupled QDs is as low as the spectral resolution of our spectrometer, 40 μeV , a value comparable to the smallest linewidth reported so far (6). The decrease of the exciton lifetime for the antibonding state with increasing level separation can be described in a simple two-level picture involving acoustical phonon scattering from the upper state into the lower state (19). This would lead to a cubic dependence of this linewidth on the energy level separation, which is also observed experimentally.

CEO has proven to be a versatile method for the fabrication of zero-dimensional objects of well-defined size, shape, and position. The excellent optical quality, manifested in extremely narrow emission lines, and the high degree of homogeneity accessible with this method permit the precise tailoring of the quantum-mechanical coupling between these nanoscale structures. As an extension to this work, we propose the use of higher barriers, narrower QWs, and the incorporation of indium into the wells. All these measures should increase the binding energy of excitons to the QDs. The use of strained InGaAs QWs, in particular, is expected to enhance this binding energy drastically because the strain can be almost completely elastically relaxed at the interfaces. This might open a route to experimental investigation of a variety of quantum mechanics textbook examples previously inaccessible by other means, such as going from artificial atoms to molecules to an artificial one-dimensional solid.

same objective lens and directed to a confocal imaging system, which defined a nearly diffraction-limited detection range of FWHM ≈ 800 nm. The PL signal was dispersed with a triple-grating spectrometer (spectral resolution = 40 μeV) and detected with a cooled charge-coupled-device camera.

16. The PL energy of (110) QWs is red-shifted with respect to that of (001) QWs of identical thickness because of different heavy hole masses in these two directions.
17. J. Hasan et al., *Nature* **380**, 54 (1997).
18. M. Grundmann and D. Bimberg, *Phys. Rev. B* **55**, 4054 (1997).
19. P. Platzman, personal communication.
20. Y. C. Chang, L. L. Chang, L. Esaki, *Appl. Phys. Lett.*

- 47, 1324 (1985).
21. A. R. Göni et al., *ibid.* **61**, 1958 (1992).
22. W. Wegschälder et al., *Phys. Rev. Lett.* **71**, 4071 (1993).
23. T. Someya, H. Akiyama, H. Sakaki, *ibid.* **74**, 3654 (1995); *ibid.* **78**, 2966 (1996).
24. W. Wegschälder, G. Schedelbeck, G. Abstreiter, M. Rother, M. Bichler, *ibid.* **78**, 1817 (1997).
25. We thank A. Zrenner for helpful discussions. Supported by the Deutsche Forschungsgemeinschaft in the framework of SFB-348 and the Bundesministerium für Bildung, Wissenschaft, Forschung, und Technologie through contract 01 BM 630/1.

13 August 1997; accepted 15 October 1997

Organically Modified Aluminosilicate Mesostructures from Block Copolymer Phases

Markus Templin, Achim Franck, Alexander Du Chesne, Heike Leist, Yuanming Zhang, Ralph Ulrich, Volker Schädler, Ulrich Wiesner*

Organically modified aluminosilicate mesostructures were synthesized from two metal alkoxides with the use of poly(isoprene-*b*-ethyleneoxide) block copolymers (PI-*b*-PEO) as the structure-directing molecules. By increasing the fraction of the inorganic precursors with respect to the polymer, morphologies expected from the phase diagrams of diblock copolymers were obtained. The length scale of the microstructures and the state of alignment were varied using concepts known from the study of block copolymers. These results suggest that the use of higher molecular weight block copolymer mesophases instead of conventional low-molecular weight surfactants may provide a simple, easily controlled pathway for the preparation of various silica-type mesostructures that extends the accessible length scale of these structures by about an order of magnitude.

REFERENCES AND NOTES

1. K. Brunner et al., *Phys. Rev. Lett.* **68**, 3216 (1992).
2. N. C. van der Vaert et al., *ibid.* **74**, 4702 (1995); F. R. Waugh et al., *ibid.* **75**, 705 (1995).
3. A. Zrenner et al., *ibid.* **72**, 3382 (1994).
4. H. F. Hess, E. Batzig, T. D. Harris, L. N. Pfeiffer, K. W. West, *Science* **264**, 1740 (1994).
5. K. Brunner, G. Abstreiter, G. Böhm, G. Tränkle, G. Weimann, *Phys. Rev. Lett.* **73**, 1138 (1994).
6. D. Gammon, E. S. Snow, B. V. Shanabrook, D. S. Kratzar, D. Park, *ibid.* **78**, 3005 (1995); *Science* **273**, 87 (1996).
7. J.-Y. Marzin, J.-M. Gérard, A. Izuel, D. Barier, G. Bastard, *Phys. Rev. Lett.* **73**, 718 (1994).
8. R. Leon, P. M. Petroff, D. Leonard, S. Fafard, *Science* **257**, 1868 (1995).
9. M. Grundmann et al., *Phys. Rev. Lett.* **74**, 4043 (1995).
10. M. A. Kastner, *Phys. Today* **46**, 24 (January 1993); O. Kohn et al., *Phys. Rev. Lett.* **74**, 785 (1995); R. C. Ashoori et al., *ibid.* **71**, 613 (1993); R. C. Ashoori, *Nature* **379**, 413 (1996).
11. S. Tarucha, D. G. Austing, T. Honda, R. J. van der Hage, L. P. Kouwenhoven, *Phys. Rev. Lett.* **77**, 3613 (1996).
12. Y. Arakawa and A. Yariv, *IEEE J. Quantum Electron.* **22**, 1887 (1986).
13. L. Kouwenhoven, *Science* **268**, 1440 (1995).
14. L. Pfeiffer et al., *Appl. Phys. Lett.* **58**, 1697 (1990).
15. Light from a tunable dye laser was focused through a microscope objective lens (numerical aperture = 0.75, power density = 50 W cm⁻²) onto the sample mounted in a He cryostat. Under such conditions, less than one exciton at a time is expected to be in the QDs. The emitted light was collected by the

Currently, a great deal of attention is being paid to the synthesis of complex inorganic materials with long-range order (1). Such materials could find applications in catalysis, membrane and separation technology, and molecular engineering (2). A typical approach is the use of organic structures formed through self-assembly as structure-directing agents. The final morphology is then determined by the cooperative organization of inorganic and organic molecular species into three-dimensionally structured arrays, a concept also discussed in the context of biomineralization (3). This strategy has already been successfully used in the preparation of inorganic mesoporous materials (4). Different pathways, where the driving forces of the cooperative organization are either ionic (5) or based on hydrogen bonds (6), have been described in vastly different concentration regimes (7). Pore sizes of 20 to 100 Å are commonly obtained in this way.

Here, we used block copolymers of high-

er molecular weight to make the transition from the small to the large mesoscopic regime (up to several tens of nanometers) of silica-type mesostructures. Bagshaw et al. previously used block-type low-molecular weight surfactants as templating agents to produce mesoporous molecular sieves (6). Higher molecular weight block copolymers have been used to stabilize inorganic metal or semiconductor nanoparticles (8). However, they all produce solid particles with morphologies never very far from spherical (9). An example of a different shape of inorganic material in a random-coil organic homopolymer is the synthesis of randomly distributed inorganic nanowires (10). Most recently, block copolymers have been used to control the growth of anisotropic inorganic crystals (11).

Block copolymer materials are similar to low-molecular weight nonionic surfactant solutions with respect to their general phase behavior (12). The phase diagrams of these materials have been elucidated by numerous experimental and theoretical studies (13). The combination of inorganic siliceous components in a hybrid material with block copolymers is appealing for various reasons.

Max-Planck-Institut für Polymerforschung, Postfach 3148, 55021 Mainz, Germany.

*To whom correspondence should be addressed.

First, a blend of desirable macroscopic properties (mechanical, thermal, and so forth) in the final product can be expected. Because the block copolymer chemistry (architecture, chain length, composition, and so forth) can be varied substantially, it should be possible to fine tune the properties of the composite. Moreover, the length scale of the microstructures of block copolymers is on the order of the characteristic length scale of the chains, ranging from 5 to 100 nm, which may make mesoporous materials with large pore sizes accessible. We investigated the sol-gel process of a mixture of two metal alkoxides, (3-glycidyloxypropyl)-trimethoxysilane, $(\text{CH}_3\text{O})_3\text{Si}(\text{CH}_2)_3\text{OCH}_2\text{CHCH}_2\text{O}$ (GLYMO), and aluminum sec-butoxide, $\text{Al}(\text{OBu}^i)_3$, with poly(isoprene-*b*-ethylene-oxide) block copolymers (PI-*b*-PEO) (Fig. 1). GLYMO itself is an interesting hybrid material known to form thin-film coatings on polymers, thereby enhancing the abrasion resistance up to values of conventional glass (14). The block copolymer has two important features. First, the hydrolysis products of the metal alkoxides should preferentially swell the hydrophilic PEO block as a result of hydrogen bonding (as known, for example, from the synthesis of mesoporous molecular sieves with low-molecular weight nonionic surfactants) (6, 7). Second, the low glass transition temperature $T_g \approx 213$ K of the PI block introduces high mobility at ambient temperatures and should allow rapid formation of structures with long-range order even in the bulk.

Two PI-*b*-PEO block copolymers, referred to as PP3 and PP7, were synthesized by anionic polymerization using a recently described procedure (15). The molecular weights are nearly 10 kg mol^{-1} (PP3) and 34 kg mol^{-1} (PP7), and the polydispersity is low ($M_w/M_n \approx 1.05$, where M_w and M_n are the weight-average and number-average molecular weights, respectively). The volume fraction of the PEO block is $\sim 15\%$ in both cases. Their microdomain structure

was explored by small-angle x-ray scattering (SAXS) (Fig. 2). In a representative SAXS pattern obtained for PP3 at room temperature (Fig. 2A), the main peak is centered around a value for the scattering wave vector q corresponding to ~ 11.9 nm. There are at least two higher order reflections clearly visible at angular positions of $\sqrt{2}$ and $\sqrt{3}$ of the first-order maximum. This pattern is characteristic for spheres packed in a simple or body-centered cubic lattice, as expected for this volume fraction.

In a typical preparation of an organic-inorganic composite, 0.5 g of PI-*b*-PEO block copolymer was dissolved in a 1:1 mixture of CHCl_3 and tetrahydrofuran (5 weight % polymer); under moderate stirring, a pre-hydrolyzed solution of 80 mol % GLYMO and 20 mol % $\text{Al}(\text{OBu}^i)_3$ (16) was added, and after 2 hours the mixture was transferred to a petri dish at 333 to 343 K. After subsequent evaporation of the organic solvents (~ 1 hour), the formation of the composite was accomplished by heat treatment at 403 K in vacuum for 45 min. A series of film samples with thicknesses of ~ 0.5 to 1 mm were prepared in this way by adding different amounts of the metal alkoxide solution to the same block copolymer. In the following, we focus on samples with 0.22 and 0.57 g of metal oxides in 0.5 g of PP3, denoted PP3/4 and PP3/10, respectively.

In the SAXS pattern of PP3/4 (Fig. 2B), the main peak is located at a q value corresponding to ~ 20.3 nm, and there are higher order reflections at angular positions of $\sqrt{4}$ and $\sqrt{7}$ of this first-order maximum. This spacing sequence is indicative of a hexagonal array of cylinders. For PP3/10 (Fig. 2C), the main peak is centered around a q value corresponding to ~ 19.6 nm, and two more reflections of higher order are clearly visible at integer multiples of this q value. Such a sequence is characteristic of an arrangement of lamellae.

To corroborate the assignment of these two SAXS patterns to a cylindrical and a lamellar morphology, respectively, we also examined the samples by transmission electron microscopy (TEM) (Fig. 3). The contrast in these micrographs arises from PI, stained with OsO_4 , and appearing black. The image of PP3/4 (Fig. 3A) clearly shows hexagonally packed cylinders in the two most typical projections. The TEM image of PP3/10 (Fig. 3B) exhibits lamellae. To determine whether the silica-type material is confined to one phase of the block copolymer, we used the recently developed method of elemental mapping (17). In Fig. 3C the silicon map of the same area depicted in Fig. 3B is shown; areas containing silicon appear bright in this image. Two conclusions can be drawn from Fig. 3C: (i) The inorganic silicon-rich phase

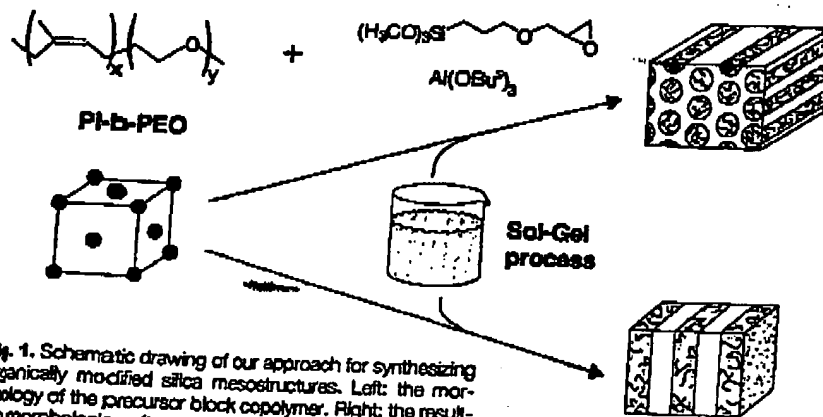


Fig. 1. Schematic drawing of our approach for synthesizing organically modified silica mesostructures. Left: the morphology of the precursor block copolymer. Right: the resulting morphologies after addition of various amounts of the metal alkoxides.

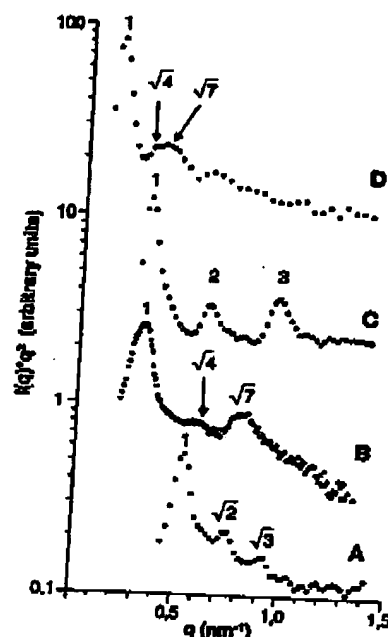


Fig. 2. Scattered intensities $I(q)$ as a function of scattering vector q for PP3 (A), PP3/4 (B), PP3/10 (C), and PP7/4 (D) at 295 K. Angular positions of higher order peaks with respect to the first-order maximum are indicated for each curve. The maxima with an angular position of $\sqrt{3}$, usually expected for a cylindrical morphology, are not well resolved in curves (B) and (D), probably because of the large width of the peaks. The patterns in (A), (C), and (D) were obtained with a Kratky compact camera (Anton Paar KG) equipped with a one-dimensional position-sensitive detector (M. Braun). The Ni-filtered Cu K α radiation ($\lambda = 0.154$ nm) was from a Siemens generator (Kristalloflex 710 H) operating at 35 kV and 30 mA. The pattern in (B) was obtained with a Rigaku Rotaflex x-ray source and a 2D area detector after integration over the azimuthal angle (see Fig. 4).

has a lamellar morphology, and (ii) comparison of Fig. 3B and Fig. 3C shows that silicon is confined to the PEO phase of PP3. The

same spatial distribution can be shown by aluminum mapping, and similar results were obtained for the hexagonal phase (18).

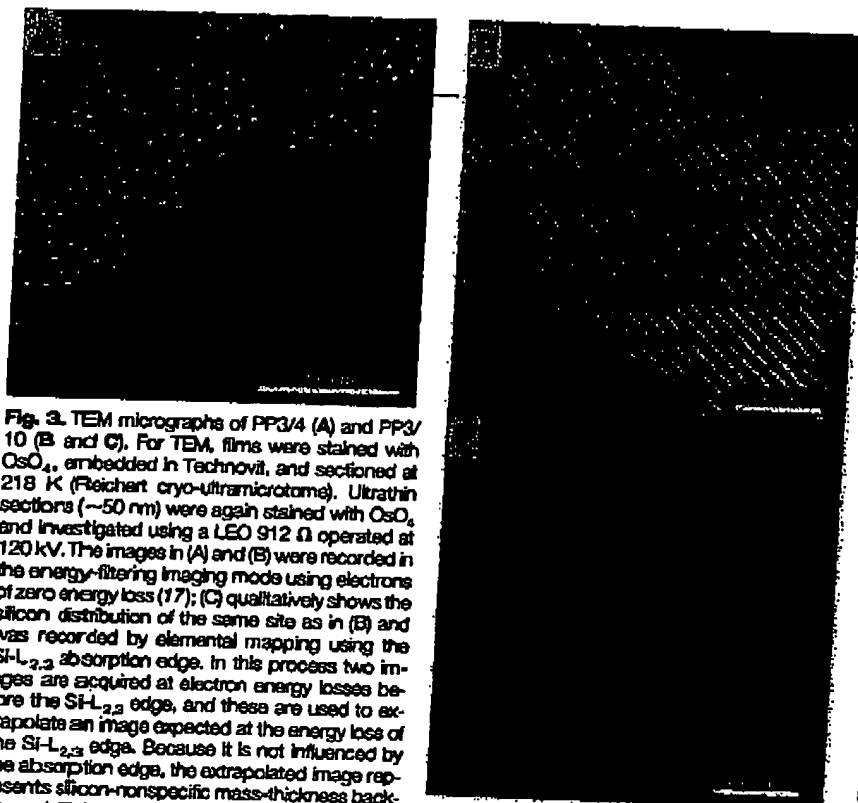


Fig. 3. TEM micrographs of PP3/4 (A) and PP3/10 (B and C). For TEM, films were stained with OsO_4 , embedded in Technovit, and sectioned at 218 K (Reichert cryo-ultramicrotome). Ultrathin sections (~ 50 nm) were again stained with OsO_4 and investigated using a LEO 912 Ω operated at 120 kV. The images in (A) and (B) were recorded in the energy-filtering imaging mode using electrons of zero energy loss (17); (C) qualitatively shows the silicon distribution of the same site as in (B) and was recorded by elemental mapping using the $\text{Si-L}_{2,3}$ absorption edge. In this process two images are acquired at electron energy losses before the $\text{Si-L}_{2,3}$ edge, and these are used to extrapolate an image expected at the energy loss of the $\text{Si-L}_{2,3}$ edge. Because it is not influenced by the absorption edge, the extrapolated image represents silicon-nonspecific mass-thickness background. This background is then subtracted from a third image acquired at the $\text{Si-L}_{2,3}$ edge, the difference image representing the pure distribution of silicon to the contrast (24). The smaller distance in the lamellar spacing in the TEM images relative to that indicated by the SAXS data is a result of contraction of the ultrathin sections normal to the plane of the lamellae, driven by free energy minimization (25).

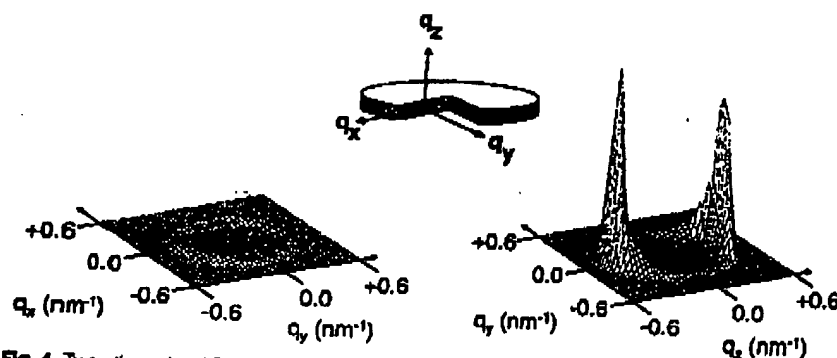


Fig. 4. Two-dimensional SAXS patterns of PP3/10 at 295 K for two different directions of the x-ray beam with respect to the sample coordinate frame, as schematically depicted in the inset. The order parameter (P_2) for the angular distribution of the lamellae normal with respect to the z-direction (film-normal), as obtained from the 2D SAXS pattern (21) on the right side, is 0.5. Patterns were obtained with a Rigaku Rotaflex x-ray source at 0.154 nm (Cu K α). A three-pinhole collimator was used to generate a beam 1 mm in diameter. Scattering patterns were recorded on a 2D Siemens X-1000 area detector with a sample-to-detector distance of 130 cm.

The length scale of the morphologies in the present composites reflected from the SAXS patterns in Fig. 2, B and C, is ~ 20 nm, considerably longer than what is typically obtained for materials prepared from low-molecular weight surfactants. The spacings can be further increased by using higher molecular weight block copolymers. In composites prepared from PP7, spacings of ~ 40 nm were achieved (Fig. 2D). Because molecular weights of up to 10^2 to 10^3 kg mol $^{-1}$ can be synthesized, fine-tuning of morphological parameters becomes possible.

The electron microscopy results (Fig. 3) suggest that the hydrophilic PEO block acts as an anchor for the metal alkoxide condensation products. More information about this effect was obtained from differential scanning calorimetry (DSC) (19). Although the T_m value of the PI block is unaffected, the melting behavior of the PEO block is markedly altered by the addition of inorganic material (18). For pure PP3, a melting point T_m was clearly detected at 310 K. For samples PP3/4 and PP3/10, however, the crystallization of the PEO block was suppressed. This is a well-known phenomenon in polymer blending, where the intimate mixing of a second polymer prevents PEO crystallization (20). Crystallization is only suppressed, however, if during the synthesis the organic solvents are evaporated at temperatures above the T_m of PEO. This suggests that the PEO chains and the hydrolysis products of the metal alkoxides mix well only above the T_m of the PEO block, and this state is frozen through condensation of the metal alkoxides.

Information about the inorganic connectivities can be gained by solid-state nuclear magnetic resonance. The condensation behavior of the present mixtures is similar to that of the pure metal alkoxides (21). Most of the silicon atoms are connected to two or three other metal atoms (silicon or aluminum) by oxygen bridges, thereby yielding a three-dimensional network. Nearly 40% of the aluminum is incorporated in this network as fourfold coordinated species. The residual aluminum is located in aluminum oxohydroxo complexes, $\text{AlO}_2(\text{OH})$, $(\text{H}_2\text{O})_x$, as sixfold coordinated aluminum. In addition to the links on the inorganic side, the conversion of the epoxy group to oligoethyleneoxide derivatives leads to a higher network density.

Finally, we concentrate on orientational effects induced by the solvent-cast technique (22), which is part of the preparation procedure for our materials. Two-dimensional (2D) SAXS patterns for two different orientations of a film of lamellar sample PP3/10 with respect to the x-ray beam (Fig. 4) show that in the q_x - q_y plane (film plane) only a ring of small scattering intensity is

observed, whereas in the q_x - q_y plane two strong and narrow scattering peaks along q_x are detected. This result is expected for lamellae oriented parallel to the film surface. It demonstrates that the solvent-cast technique is capable of inducing macroscopically aligned samples for the present lamellar silica-type mesostructures. Because the film thickness of these materials is considerable (~ 1 mm), surface-induced morphological transitions and related effects observed for very thin films (23) can be neglected.

REFERENCES AND NOTES

1. M. Antonietti and C. Göthner, *Angew. Chem.* 109, 844 (1997); S. Mann and G. Ozin, *Nature* 382, 313 (1996); P. Behrens, *Adv. Mater.* 5, 127 (1993).
2. L. Mercier and T. J. Pinnavaia, *Adv. Mater.* 9, 500 (1997); F. Schüth, *Ber. Bunsenges. Phys. Chem.* 99, 1805 (1995).
3. S. Mann, *Nature* 365, 499 (1993); B. R. Heywood and S. Mann, *Adv. Mater.* 6, 9 (1994).
4. C. T. Kresge, M. E. Leonowicz, W. J. Roth, J. C. Vartuli, J. S. Beck, *Nature* 359, 710 (1992); N. K. Raman, M. T. Anderson, C. J. Einker, *Chem. Mater.* 8, 1682 (1996).
5. Q. Huo et al., *Nature* 368, 317 (1994); Q. Huo, D. I. Margolese, G. D. Stucky, *Chem. Mater.* 8, 1147 (1996); Q. Huo, R. Leon, P. M. Petroff, G. D. Stucky, *Science* 268, 1324 (1995); A. Frouzi et al., *ibid.* 267, 1139 (1995).
6. S. A. Bagshaw, E. Prouzet, T. J. Pinnavaia, *Science* 269, 1242 (1995).
7. A. Frouzi, F. Aul, A. G. Oerli, G. D. Stucky, B. F. Chmelka, *J. Am. Chem. Soc.* 119, 3596 (1997); G. S. Attard, J. C. Glyde, C. G. Göthner, *Nature* 378, 388 (1995).
8. V. Sankaran, C. C. Cummins, R. R. Schrock, R. E. Cohen, R. J. Sibey, *J. Am. Chem. Soc.* 112, 6858 (1990); Y. N. G. Chen, R. R. Schrock, R. E. Cohen, *Chem. Mater.* 4, 24 (1992); M. Moffitt, L. McMahon, V. Pessot, A. Eisenberg, *ibid.* 7, 1195 (1995); J. P. Spatz, A. Roscher, S. Shinko, G. Krausch, M. Möller, *Adv. Mater.* 7, 731 (1995); M. Antonietti, E. Wenz, L. Bronstein, M. Seregna, *ibid.*, p. 1000; R. T. Clay and R. E. Cohen, *Supramol. Sci.* 2, 183 (1996); R. S. Kane, R. E. Cohen, R. Sibey, *Chem. Mater.* 8, 1919 (1996).
9. P. V. Braun, P. Osener, S. I. Stupp, *Nature* 380, 825 (1998).
10. J. H. Golden et al., *Science* 273, 782 (1996).
11. J. M. Maremonte, J. Norwig, E. Stöckmann, W. H. Meyer, G. Wagner, *Adv. Mater.* 9, 647 (1997).
12. M. A. Hämmer et al., *Science* 271, 976 (1996).
13. F. S. Bates, *ibid.* 261, 898 (1991).
14. H. Schmidt and H. Wöhrer, *J. Non-Cryst. Solids* 121, 428 (1990).
15. J. Allgauer, A. Poppa, L. Wilner, D. Richter, *Macromolecules* 30, 1582 (1997).
16. The prehydrolyzed sol was prepared by mixing GLYMO and $\text{Al}(\text{OEt})_3$ at 273 K and adding 16% of the stoichiometric amount of water required for the complete hydrolysis of the metal alkoxide groups. The water contained HCl in a molar ratio (relative to the metal alkoxides) of 3.6×10^{-6} . After 15 min of stirring, the temperature was raised to 295 K. After a further 15 min, the residual water for the complete hydrolysis of the alkoxide groups was added, and the mixture was stirred for 1 hour and then poured into the block copolymer solution.
17. L. Ratner, *Adv. Electron. Electron Phys.* 81, 67 (1991).
18. M. Templin, A. Franck, A. Du Chesne, H. Leist, Y. Zhang, R. Ulrich, V. Schädler, U. Wiesner, data not shown.
19. DSC measurements were performed on a Mettler DSC-30 with a heating rate of 10 K min^{-1} . Evaluation of the DSC curves was performed with a program from the same company.
20. S. Krause, in *Polymer Blends*, D. R. Paul and S. Newman, Eds. (Academic Press, New York, 1978), vol. 1, pp. 18-113; L. Robeson, in *Polymer Compatibility and Incompatibility*, K. Solc, Ed. (NMI Press Symposium Series, Harwood Academic, New York, 1982), vol. 2, pp. 177-211.
21. M. Templin, U. Wiesner, H. W. Spiess, *Adv. Mater.* 9, 814 (1997).
22. T. Hashimoto, K. Negatoshii, A. Toda, H. Hasegawa, H. Kawai, *Macromolecules* 7, 364 (1977); D. Ehlich, M. Takenaka, S. Okamoto, T. Hashimoto, *ibid.* 26, 189 (1993); C. C. Honaker and E. L. Thomas, *Chem. Mater.* 8, 1702 (1996).
23. Y. Liu, M. H. Rafailovich, J. Sokolov, S. A. Schwarz, S. Balal, *Macromolecules* 29, 899 (1996); G. Coulon, T. P. Russell, V. R. Deline, P. F. Green, *ibid.* 22, 2581 (1989); C. S. Henke, E. L. Thomas, L. J. Fetters, *J. Mater. Sci.* 23, 1885 (1988).
24. A. Du Chesne, G. Lissar, G. Wagner, *Colloid Polym. Sci.* 272, 1329 (1994); A. Du Chesne, K. Wenke, G. Lissar, G. Wenz, *Acta Polym.* 48, 142 (1997).
25. The decrease of the lamellar spacing is exclusively attributable to convex bending of the liquid-like lamellar surface. Two driving forces must be considered: surface tension (up to a critical ratio of lamella thickness to section thickness, the free lamella surface decreases upon bending) and entropy (partial relaxation of entropically unfavorable chain conformation [stretched chains in lamellae in bulk]). For details, see A. Du Chesne, thesis, University of Mainz (1993).
26. We thank H. W. Spiess for his strong support of this work, T. Thum-Albrecht for help in performing SAXS measurements and for fruitful discussions, and U. Pawelzik for performing the DSC measurements. M.T. thanks the Bundesministerium für Bildung, Wissenschaft, Forschung und Technologie (project BS N 100900) for financial support.

8 July 1997; accepted 23 October 1997

Promotion of the Cycling of Diet-Enhancing Nutrients by African Grazers

S. J. McNaughton,* F. F. Banyikwa, M. M. McNaughton

Experiments in Serengeti National Park, Tanzania, provide direct evidence that large, free-ranging mammalian grazers accelerate nutrient cycling in a natural ecosystem in a way that enhances their own carrying capacity. Both nitrogen and sodium were at considerably higher plant-available levels in soils of highly grazed sites than in soils of nearby areas where animal density is sparse. Fencing that uncoupled grazers and soils indicated that the animals promote nitrogen availability on soils of inherently similar fertility and select sites of higher sodium availability as well as enhancing that availability.

There is a growing recognition in ecology that organisms can modify their environments in ways beneficial to themselves, rather than inevitably causing environmental deterioration (1), and it is a maxim of grassland ecology that nutrient recycling by grazers contributes to plant regrowth potential (2). However, direct evidence of the effect of large wild mammals on nutrient recycling is meager (3), and studies in boreal forests (4) indicate that moose (*Alces alces*) browsing indirectly diminishes soil mineralization rate by shifting the composition of vegetation species to less palatable and less decomposable plants.

The distribution and abundance of large grazing mammals in Serengeti National Park, Tanzania, are influenced by the occurrence of nutritionally sufficient forages (5) and the spatiotemporal variation of vegetation productivity due to pronounced

geographic rainfall gradients and production seasonality (6). Grazers preferentially forage on swards enriched in minerals that are important in late-stage pregnancy, lactation, and the growth of young animals (5). There are two plausible explanations for this phenomenon: Animals forage on vegetation supported by soils of innately greater nutrient availability, or animal activities augment nutrient availability. Identification of the correct explanation has implications for conservation policy and management (through an understanding of the habitat requirements of endangered wild grazing mammals) and for ecological theory (by documenting how grazing mammals are mechanistically coupled with their habitats). Regional edaphic differences affect the mineral contents of forages and thereby influence seasonal movements of migratory grazers in the Serengeti, but no evidence of general soil differences was found in landscape-level studies of resident grazers (5), which are those that do not migrate but occupy discrete home ranges. Here we present evidence concerning the mechanisms associated with higher nutrient availability at sites preferred by resident grazers.

Mineralization of two elements—nitrogen (N), which is essential to both plants

S. J. McNaughton and M. M. McNaughton, Biological Research Laboratories, Syracuse University, Syracuse, NY 13244-1220, USA; and Serengeti Wildlife Research Centre, Post Office Box 661, Arusha, Tanzania. F. F. Banyikwa, Department of Botany, University of Dar es Salaam, Post Office Box 35060, Dar es Salaam, Tanzania; Biological Research Laboratories, Syracuse University, Syracuse, NY 13244-1220, USA; and Serengeti Wildlife Research Centre, Post Office Box 661, Arusha, Tanzania.

*To whom correspondence should be addressed; E-mail: sjmcsaug@mailbox.syr.edu

**This Page is Inserted by IFW Indexing and Scanning
Operations and is not part of the Official Record**

BEST AVAILABLE IMAGES

Defective images within this document are accurate representations of the original documents submitted by the applicant.

Defects in the images include but are not limited to the items checked:

- ☐ **BLACK BORDERS**
- ☐ **IMAGE CUT OFF AT TOP, BOTTOM OR SIDES**
- ☐ **FADED TEXT OR DRAWING**
- ☐ **BLURRED OR ILLEGIBLE TEXT OR DRAWING**
- ☐ **SKEWED/SLANTED IMAGES**
- ☐ **COLOR OR BLACK AND WHITE PHOTOGRAPHS**
- ☐ **GRAY SCALE DOCUMENTS**
- ☐ **LINES OR MARKS ON ORIGINAL DOCUMENT**
- ☐ **REFERENCE(S) OR EXHIBIT(S) SUBMITTED ARE POOR QUALITY**
- ☐ **OTHER:** _____

IMAGES ARE BEST AVAILABLE COPY.

As rescanning these documents will not correct the image problems checked, please do not report these problems to the IFW Image Problem Mailbox.